metals

Article

Experimental Study on Mechanical Properties of Shear Square Section Steel Tube Dampers

Li Xiao [1], Yonggang Li [2], Cun Hui [2,*], Zhongyi Zhou [3] and Feng Deng [2]

1 CNOOC Petroleum and Gas Power Group Co., Ltd., Beijing 100020, China; xiaoli6@cnooc.com.cn
2 School of Architecture and Civil Engineering, Zhongyuan University of Technology, Zhengzhou 450007, China; 2020009306@zut.edu.cn (Y.L.); fengdeng@zut.edu.cn (F.D.)
3 Key Laboratory of Earthquake Engineering and Engineering Vibration, Institute of Engineering Mechanics, China Earthquake Administration, Harbin 150080, China; zhouzy@iem.ac.cn
* Correspondence: hcun@zut.edu.cn

Abstract: Based on the excellent performance of shear metal dampers in building seismic capacity, the traditional shear metal damper was optimized. A double-sided shear steel tube damper with simple structure, easy replacement, and wide application is proposed. In order to study the influence of different design parameters on its seismic performance, taking the steel tube length, height, width, thickness, and connection mode as variables, five groups of 15 specimens were designed for experimental research, and the failure modes, characteristic loads and displacements, hysteretic curves, skeleton curves, stiffness degradation curves, and energy dissipation capacity of each specimen were analyzed in detail. The test results showed that the hysteretic curves of each specimen were full and that the energy dissipation capacity was good. The greater the thickness of the steel tube was, the greater the load-bearing capacity of the damper and the larger the hysteresis loop area were. The greater the width of the steel tube was, the greater the equivalent stiffness was. As displacement amplitude increased, the equivalent stiffness of the specimen showed a downward trend. The two connection modes had their own advantages and disadvantages, and a damper with reasonable connection form would need to be selected according to actual engineering needs.

Keywords: shear dampers; steel tube dampers; low cycle cyclic load; mechanical properties; energy dissipation capacity

check for updates

Citation: Xiao, L.; Li, Y.; Hui, C.; Zhou, Z.; Deng, F. Experimental Study on Mechanical Properties of Shear Square Section Steel Tube Dampers. *Metals* **2022**, *12*, 418. https://doi.org/10.3390/met12030418

Academic Editors: Zhihua Chen, Hanbin Ge and Siu-lai Chan

Received: 21 January 2022
Accepted: 25 February 2022
Published: 26 February 2022

1. Introduction

Shear metal dampers can consume seismic energy with plastic deformation by themselves. They can significantly enhance the comprehensive seismic capacity of high buildings. The replaceable property of the metal dampers can promote the rapid postearthquake recovery of building functions [1–4]. Traditional shear metal dampers are mainly used in high-rise or super-high-rise buildings and are not suitable for low multistory buildings because of their complex structure and high cost [5–7].

Since dampers can significantly improve the seismic capacity of buildings, many experts and scholars have studied them. Refs. [8–10] introduced the I-shaped steel damper with shear yield mechanism, which was economical and applicable, had a simple structure, and was easy to construct and replace after an earthquake, and evaluated the parameters of the proposed damper. The results showed that the I-shaped steel damper acted as a ductile fuse, which could prevent the buckling of diagonal elements of concentric braced frame systems and improve the hysteretic performance of concentric braced frames. The necessary relationship for designing this type of damper and a simple method for predicting the nonlinear behavior of the support installed with the damper and estimating the load displacement model of the damper without finite element modeling were also proposed. Lin et al. [11] developed a buckling restrained shear plate damper with removable steel–concrete composite restraint, which simplified the manufacturing process and made the limiter structure light and firm. Test results showed that the composite restraint plate of the damper effectively limited the local and overall out-of-plane deformation of the inner steel shear panel. Deng et al. [12] conducted a quasistatic test on a new buckling restrained shear plate damper (BRSPD) specimen. The results showed that a restrained plate with sufficient stiffness and strength could effectively restrain the out-of-plane buckling of the energy dissipation plate. The BRSPD was numerically analyzed by using the general finite element program. According to the test and analysis results, a design method for the restrained plate and bolt was proposed. Yao et al. [13] used a square steel tube as an out-of-plane stiffener of a steel core plate with low yield point, reduced the flange plate section to alleviate the end fracture, and used the combined hardening constitutive model with memory surface to characterize the plasticity of the square steel tube. They established a numerical model of the shear panel damper and proposed a simplified calibration method. Kamaludin et al. [14] conducted incremental dynamic analysis (IDA) of reinforced concrete frame structures with viscoelastic dampers, friction dampers, and BRB dampers, taking both far- and near-field seismic scenarios into account. The results showed that compared with other energy dissipation devices, viscoelastic dampers had better performance in reducing seismic damage. In contrast, Aydin et al. [15] considered the effect of soil–structure interaction in the optimal design of cohesive dampers and applied a damper optimization method based on the target damping ratio and interlayer displacement ratio from the literature to a building structure model considering different types of sandy soils. The first- and second-order modal responses were considered separately using the time–distance analysis method, and the results showed that the negative effects of sandy soils on the dynamic performance of the superstructure could be overcome by optimizing the dampers in the buildings. It was shown that the effect of soil should be considered when solving the damper optimization problem.

Cruze et al. [16,17] studied magnetorheological dampers with high energy dissipation capacity, low power consumption, perfect damping mechanism, good stability, and fast response time and proposed a method to generate magnetic fields using multiple coils. The magnetorheological dampers were simulated under different currents to simulate the seismic effects, and the results showed that such dampers could effectively reduce the structural response in regions of medium and high seismic activity. Numerical hybrid simulations were performed using OpenSees, and the results showed a significant reduction in displacement and an increase in energy dissipation capacity under major seismic events. Khalili et al. [18] proposed a hysteretic damper for energy dissipation of beam–column steel connections through the bending deformation of an internal hourglass-shaped steel pin. Through experiments and finite element simulations, it was shown that the damper had a high energy dissipation capacity and that the resistance did not decrease significantly during the loading cycle, which improved the ductility and seismic resilience of the whole building structure.

Several scholars have studied curved damped truss moment frame (CDTMF) systems designed using equivalent energy design methods [19,20]. The seismic performance of buildings with different story heights was evaluated using three different analysis methods: nonlinear static analysis, nonlinear time-dependent analysis, and incremental dynamic analysis, and the results showed that CDTMF had excellent ductility and energy dissipation capacity and could effectively control the top plate displacement, interstory displacement, and top plate acceleration. CDTMF could also be used as an effective seismic resisting system. Barbagallo et al. [21] proposed a design method for flexural restrained braced seismic reinforcement measures. Based on a numerical study, the parameters controlling the design method were calibrated to ensure that the near-collapse performance objectives specified in Eurocode 8 were achieved. Nuzzo et al. [22] proposed an effective and easy-to-use displacement-based procedure considering bracing flexibility for the seismic design or retrofit of frame structures with hysteresis dampers. The effectiveness of the proposed procedure was demonstrated in two case studies, for new and existing buildings, with high agreement between the analytical objectives and the numerical capacity curves. Finally, the reliability of the designed frames was evaluated by static and dynamic nonlinear analysis. Mazza [23] considered structural seismic degradation and proposed a displacement-based design (DBD) method using a hysteresis model based on plasticity and damage mechanisms to describe the inelastic response of reinforced concrete frame members. A nonlinear seismic analysis of a single-degree-of-freedom system, equivalent to a multi-degree-of-freedom model of the structure, was performed to generate capacity boundary curves using a hysteresis model defined from the initial backbone curve. Different strengthening schemes were compared, and the effects of different damage levels and different damage evolution patterns were investigated. Finally, pushover curves are calculated for unsupported and damped braced structures with and without consideration of the hysteretic response degradation of the RC frame members. Improvements will be made by inserting hysteretic damping supports to achieve the performance levels specified by the current Italian regulations in high-risk seismic zones.

Other scholars have also carried out experimental research and numerical simulations on the aspects of constitutive relationship and defect form. Golmoghany et al. [24] proposed a new hybrid control system composed of a friction damper and a vertical shear plate in series. In moderate earthquakes, the friction damper (FD) works as the first fuse, while in strong earthquakes, the FD and the vertical shear plate consume energy together. Based on a test, the model was established by software, and the results showed that the seismic effect of this hybrid damper was better than that of a standard reference. Kiani et al. [25] proposed a new type of two-stage yield vertical bar system hybrid damper. The applicability and cyclic response of the proposed system were tested by using the nonlinear finite element modeling protocol in the finite element software. The cyclic secant stiffness, energy dissipation capacity, and equivalent viscous damping ratio of the structure using the hybrid damper were significantly increased. A minimum free span height ratio was also proposed. Lin et al. [26] designed a new type of adaptive shear thickened fluid full-scale damper (STFD) and applied it to suppress the bad vibrations of cables. According to the experimental phenomenon, a phenomenon model in line with the observed performance of the STFD was proposed, the general differential equation of the cable system in the STFD was established, and the eigenvalue problem of the STFD cable system was solved by the finite difference method. This provided a tool for accurately measuring the attenuation process and damping force. Suzuki [27] proposed a method to search for the shape of defects to reproduce a target load displacement relationships and then used the modal iterative error correction method to change each modal coefficient to fit the target load displacement relationship. It was proved that the load displacement relationship of shear plate dampers could be controlled by the shape of defects. Xu et al. [28] conducted repeated load tests with load conditions and size parameters as test variables, proposed a kinematic isotropic composite hardening model, considered the loading history effect, and accurately simulated the complex hysteretic performance of significant strain hardening.

Although many experts and scholars have studied metal dampers, the form of these dampers is not simple enough and the cost is not low enough, so there is still much left to research. In this paper, traditional shear damping devices were optimized, and a kind of double-sided shear steel tube damper with low cost is proposed. The energy dissipation due to elastoplastic deformation caused by in-plane shearing of steel tube side plates was used to reduce vibration. The proposed dampers had the advantages of easy availability of materials, low cost, simple structure, and ability to be used in few-storied buildings in the areas of villages and small towns. Five groups with 15 square section seamless steel tube dampers were designed, and low-cycle repeated load tests were carried out. The influence of different design parameters on the mechanical properties of shear steel tube dampers was analyzed, and the seismic mechanism was revealed.

2. Experiments Details

The shear-type steel tube damper proposed was made of Q235 steel and consisted of steel tube, a T-shaped plate, and an L-shaped connecting plate, as shown in Figure 1.

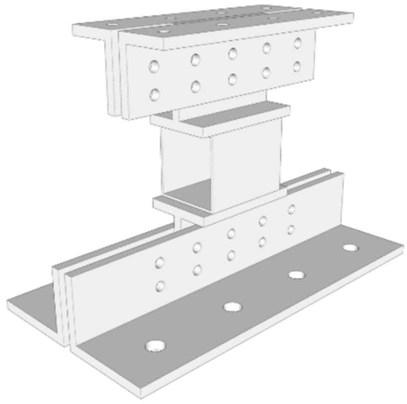

Figure 1. Schematic diagram of shear square section steel tube damper.

The upper and lower sides of the steel tube were welded to the T-shaped plate, and the L-shaped connectors were assembled to the T-shaped plate by bolts. In addition, a set of dampers connected by bolts between the steel tubes and T-shaped plate were set to study the influence of different connection modes on the mechanical properties of the dampers. The thickness of the T-shaped plate was 4 times that of the energy-dissipating part of the steel tube, which was much greater than the thickness of the steel tube. This ensured that only the energy-dissipating part of the steel tube would be consumed when the damper worked and that the steel plate connected to it remained elastic.

2.1. Design of the Specimens

The steel plates on the upper and lower sides of the shear square section steel tube damper were connected with other components by welding, and the L-shaped connector was assembled with the T-shaped plate by bolts. This constituted the nonenergy consuming part of the damper. The side steel plates bore the energy dissipation function and were the main working part of the dampers. In this paper, 5 groups of shear square section steel tube dampers were designed. Each group of dampers was designed with three widths, and the total number of specimens was 15. The influences of steel tube length L, steel tube height H, steel tube width B, steel tube thickness T, and connection mode on the shear seamless steel tube dampers with different design parameters were compared and studied. The structure is shown in Figure 2, and the design parameters are shown in Table 1. The connection forms were divided into welding and bolt connections. The effective thickness of the weld of the welded specimen was the same as that of the steel plate. The diameter of the bolt hole of the bolted specimen was 15 mm, and hexagon-head bolts were adopted.

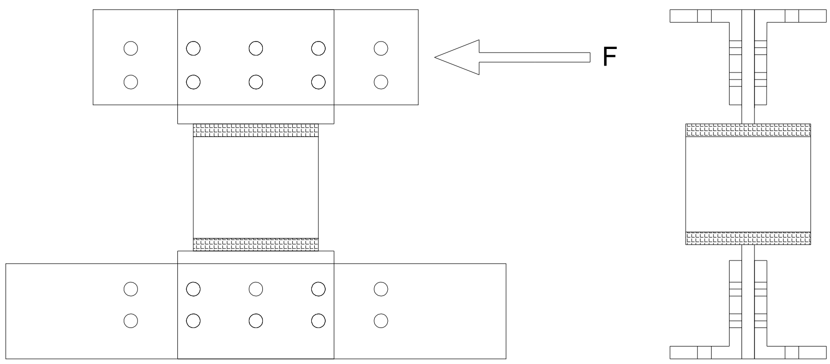

Figure 2. Structure of shear square section steel tube damper (L × H × B was 200 mm × 200 mm × 200 mm).

Table 1. Design parameters of the specimens.

Specimens	L/mm	H/mm	B/mm	t/mm	Connection Type
150-A1	150	150	150	3	Welded
150-A2	150	150	200	3	Welded
150-A3	150	150	250	3	Welded
150-B1	150	150	150	4	Welded
150-B2	150	150	200	4	Welded
150-B3	150	150	250	4	Welded
150-C1	150	150	150	5	Welded
150-C2	150	150	200	5	Welded
150-C3	150	150	250	5	Welded
150-D1	150	150	150	5	Bolted
150-D2	150	150	200	5	Bolted
150-D3	150	150	250	5	Bolted
200-A1	200	200	150	5	Welded
200-A2	200	200	200	5	Welded
200-A3	200	200	250	5	Welded

2.2. Material Characteristics

The steel used in the specimens was Q235. The standard tensile specimens were cut from the same batch of steel as the dampers. The size of the standard tensile specimens is shown in Figure 3. There were three standard tensile specimens in each group. The test results are shown in Table 2.

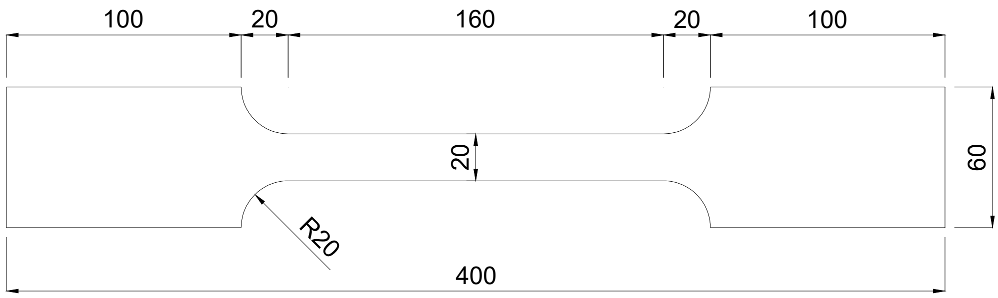

Figure 3. Drawing of standard tensile specimen (unit: mm).

Table 2. Measurement results of the steel plates.

Steel Plate	Yield Strength/MPa	Ultimate Tensile Strength/MPa	Yield Strength Ratio	Elongation/%	Elastic Modulus/MPa
3 mm	238.45	354.72	0.67	27.71	1.92 × 105
4 mm	242.08	359.76	0.67	30.43	2.12 × 105
5 mm	243.23	358.25	0.68	29.6	2.07 × 105

2.3. Loading and Measurement Scheme

The loading device is shown in Figure 4. The specimens were loaded with a displacement loading system. Suppose the yield displacement of the specimen was Δ. The target displacements of the specimens were 0.5Δ, 1Δ, 2Δ, 3Δ, 4Δ, 5Δ, 6Δ, 7Δ, 8Δ, 9Δ, and 10Δ. Each displacement was loaded 3 times until the load decreased to 85% of the ultimate load-bearing capacity. The loading scheme is shown in Figure 5.

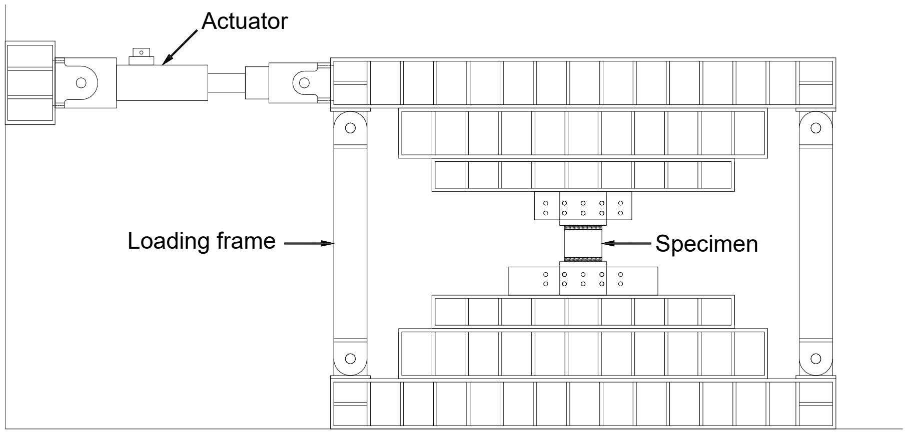

Figure 4. Loading device.

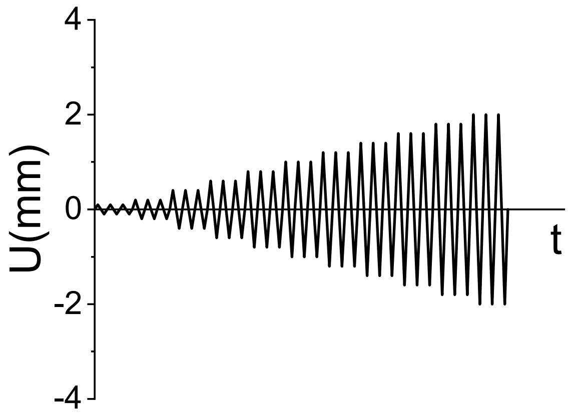

Figure 5. Loading scheme.

Displacement meters with Nos. H1, H2, H3 and H4 were set on the upper and lower sides of the T-shaped connectors and the upper and lower sides of the steel tube, respectively. A 3-directional strain was pasted on the central position of the side of the steel tube damper and an erect VIC-3D full-field strain measurement system (Beijing Reituo Technology Co., Ltd., Beijing, China) was placed on the other side of the damper. The equipment was manufactured by Beijing Reituo Technology Co., Ltd. of China. The measurement scheme is shown in Figure 6.

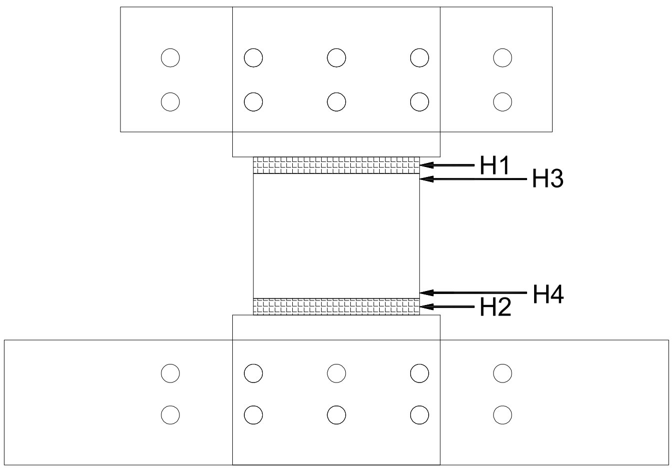

Figure 6. Measurement scheme.

3. Results and Analysis

3.1. Failure Modes

The typical failure modes of the welded steel tube dampers are shown in Figure 7, and the typical failure modes of the bolted steel tube dampers are shown in Figure 8.

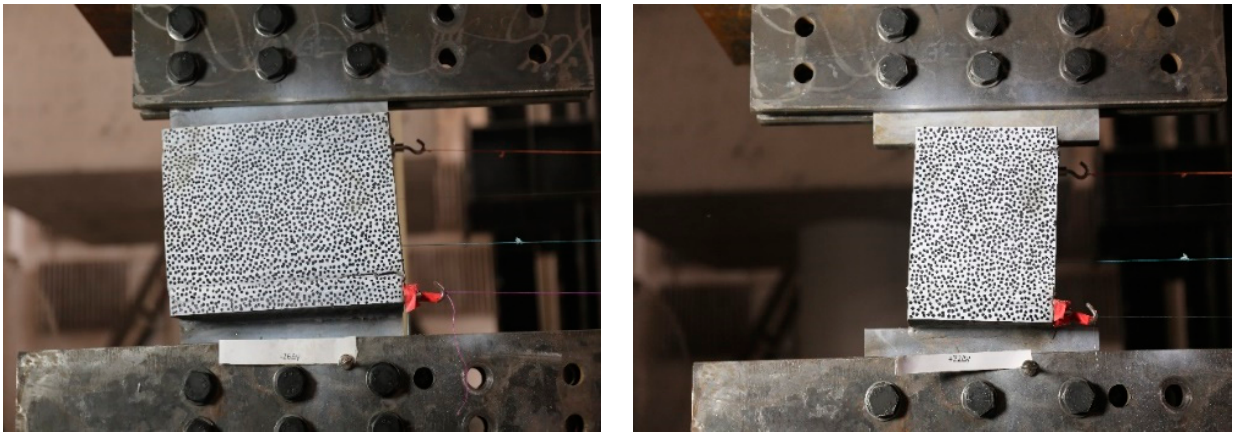

(**a**) (**b**)

Figure 7. Failure modes of the welded steel tube dampers: (**a**) steel tube end of 150-C3 tearing; (**b**) weld of 200-A1 cracking.

(**a**) (**b**)

Figure 8. Failure modes of the bolted steel tube dampers: (**a**) corner of 150-D1 warping; (**b**) steel tube end of 150-D1 tearing.

It can be observed from Figure 7 that:

1. The failure modes of welded seamless steel tube dampers were divided mainly into two types: steel tube end tearing and weld cracking.
2. Taking the specimen 150-C3 as an example, the damper had no obvious changes at the initial loading stage. With increases in displacement and load, the side of the steel tube began to tilt slightly, and the steel tube tilt became more and more obvious. When the horizontal displacement was 4.42 mm, the corresponding load was 265.92 kN, and the damper yielded with no obvious cracks. When the horizontal displacement reached 7.16 mm, the peak load-bearing capacity of the damper reached 335.80 kN. Cracks began to appear at the corner of the steel tube at last, and the damper was damaged.

It can be observed from Figure 8 that:

1. At the beginning of loading, the connection between the steel tube and the T-shaped plate became warped. With increasing displacement of the damper, the warping of the corners of the steel tube became much more obvious.

2. When the deformation of the damper was 8.08 mm, the damper began to yield, and the yield strength was 54 kN. When the relative displacement was 17.49 mm, the specimen reached to its peak load-bearing capacity, which was 64.1 kN. With increasing displacement, the bottom of the steel tube was torn, the load declined, and the damper was damaged.

3.2. Characteristic Load and Displacement

The yield displacement, peak displacement, yield load-bearing capacity, peak load-bearing capacity, and initial stiffness of the seamless steel tube dampers are listed in Table 3. The ductility coefficient is the ratio of the peak displacement to the yield displacement of the damper.

Table 3. Characteristic load and displacement of seamless steel tube dampers.

Specimens	Initial Stiffness (kN/mm)	Yield Displacement (mm)	Yield Load (kN)	Peak Displacement (mm)	Peak Load (kN)
150-A1	80.34	2.34	109.56	3.31	122.01
150-A2	114.65	1.87	162.46	2.64	174.47
150-A3	165.81	1.66	166.01	3.72	207.75
150-B1	87.60	2.72	159.99	4.86	184.18
150-B2	124.14	3.15	218.35	5.31	268.07
150-B3	180.42	4.17	269.25	7.13	339.28
150-C1	93.31	3.76	161.04	7.07	191.43
150-C2	123.75	4.84	242.03	8.35	292.92
150-C3	199.28	4.42	265.92	7.16	335.80
150-D1	13.57	8.08	53.37	17.49	64.10
150-D2	24.58	5.87	88.02	9.93	104.97
150-D3	32.15	5.15	141.90	8.45	156.17
200-A1	33.27	5.05	111.63	10.53	131.00
200-A2	56.34	5.08	175.02	9.93	203.76
200-A3	89.19	5.14	233.95	9.87	280.53

It can be observed from Table 3 that:

1. As the thickness of the damper increased, the initial stiffness gradually increased. As the width of the shear surface increased, the initial stiffness of the damper gradually increased, and the proportion of the increase was much larger.
2. The yield loads of specimens 200-A1, 200-A2, and 200-A3 were 111.63 kN, 175.02 kN, and 233.95 kN, respectively. The peak loads were 131.00 kN, 203.76 kN, and 280.53 kN, respectively. The initial stiffnesses were 33.27 kN/mm, 56.34 kN/mm, and 89.19 kN/mm, respectively. As steel tube width increased, the yield load, peak load, and initial stiffness gradually increased.
3. For the three specimens 150-A1, 150-B1, and 150-C1, the yield displacements were 2.34 mm, 2.72 mm, and 3.76 mm, respectively. The displacements corresponding to the peak loads were 3.31 mm, 4.86 mm, and 7.07 mm, respectively. The greater the thickness of the steel tube was, the greater the yield displacement and peak displacement were. The thickness had no obvious influence on the yield load, peak load, or initial stiffness, and the difference between the specimens in groups 150-B and 150-C was less than 10%.
4. By comparative analysis, the yield displacements of 150-C1 and 200-A1 were 3.76 mm and 5.05 mm, respectively, and the peak displacements were 7.07 mm and 10.53 mm, respectively. The yield loads were 161.04 kN and 111.63 kN, respectively, and the peak loads were 191.43 kN and 131.00 kN, respectively. The initial stiffnesses were 93.31 kN/mm and 33.27 kN/mm, respectively. As the height of the steel tube increased, the yield displacement and peak displacement increased by 34.48% and 48.87%, respectively, and the yield load, peak load, and initial stiffness decreased by 30.68%, 31.57%, and 64.34% respectively.

5. Comparing the welded specimen 150-C1 and the bolted specimen 150-D1, the yield displacements were 3.76 mm and 8.0 mm, respectively; the peak displacements were 7.07 mm and 17.49 mm, respectively; the yield loads were 161.04 kN and 53.37 kN, respectively; the peak loads were 191.43 kN and 64.10 kN, respectively; and the initial stiffnesses were 93.31 kN/mm and 13.57 kN/mm, respectively. Compared with the bolted specimen 150-D1, the yield displacement and peak displacement of the welded specimen 150-C1 were increased by 115.02% and 147.21%, respectively, and the yield load, peak load, and initial stiffness were decreased by 66.86%, 66.51%, and 86.45% respectively. The results showed that the welded damper had better yield load, peak load, and initial stiffness, but the bolted damper had greater yield displacement and peak displacement. Therefore, it is necessary to select a reasonably sized damper according to the actual engineering requirements.

3.3. Hysteretic Curves

The hysteretic curve, which is the relation curve between the load and displacement of a specimen, can reflect the deformation characteristics and energy dissipation capacity of the specimen. The hysteretic curves of each specimen are shown in Figure 9.

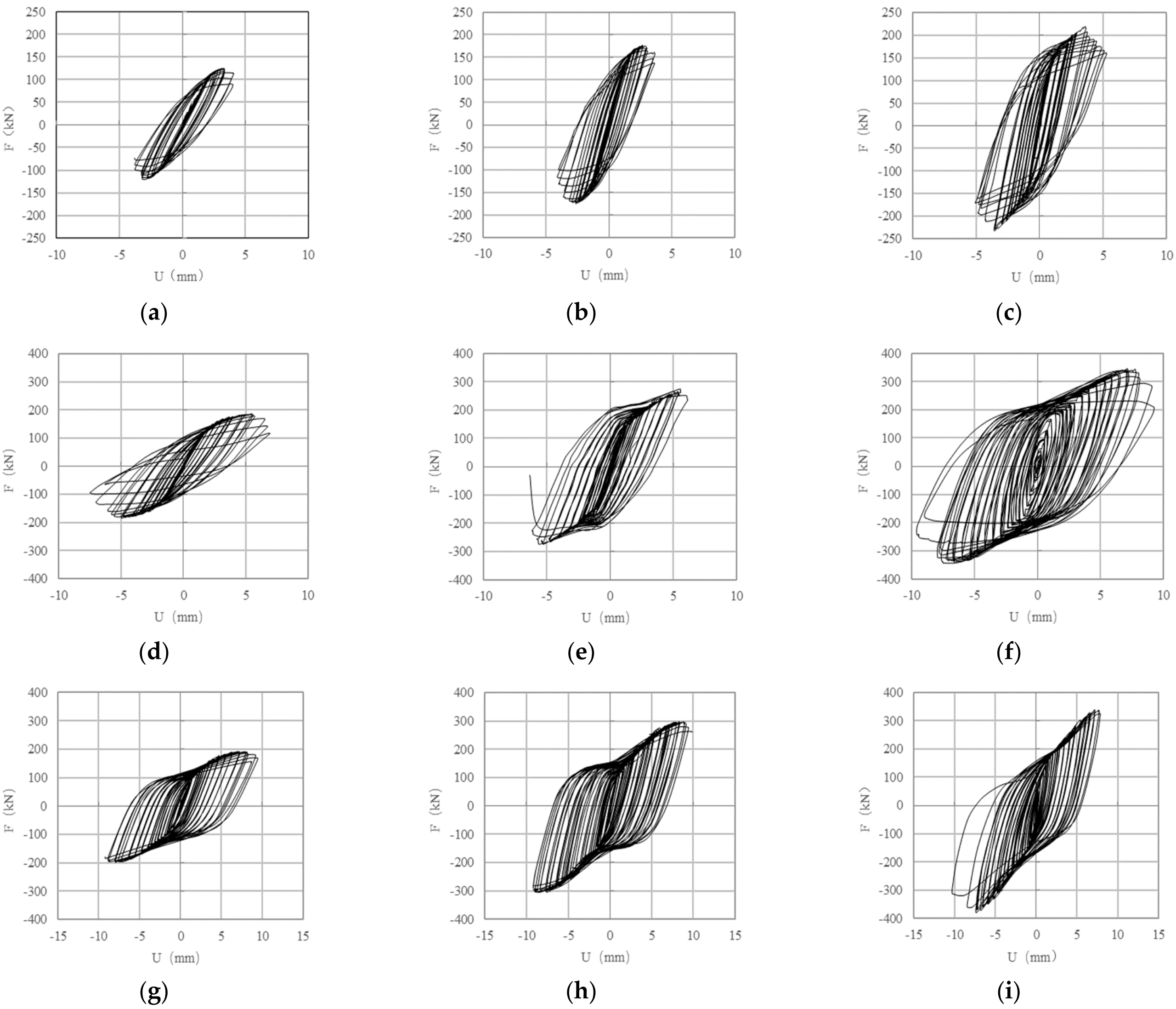

Figure 9. *Cont.*

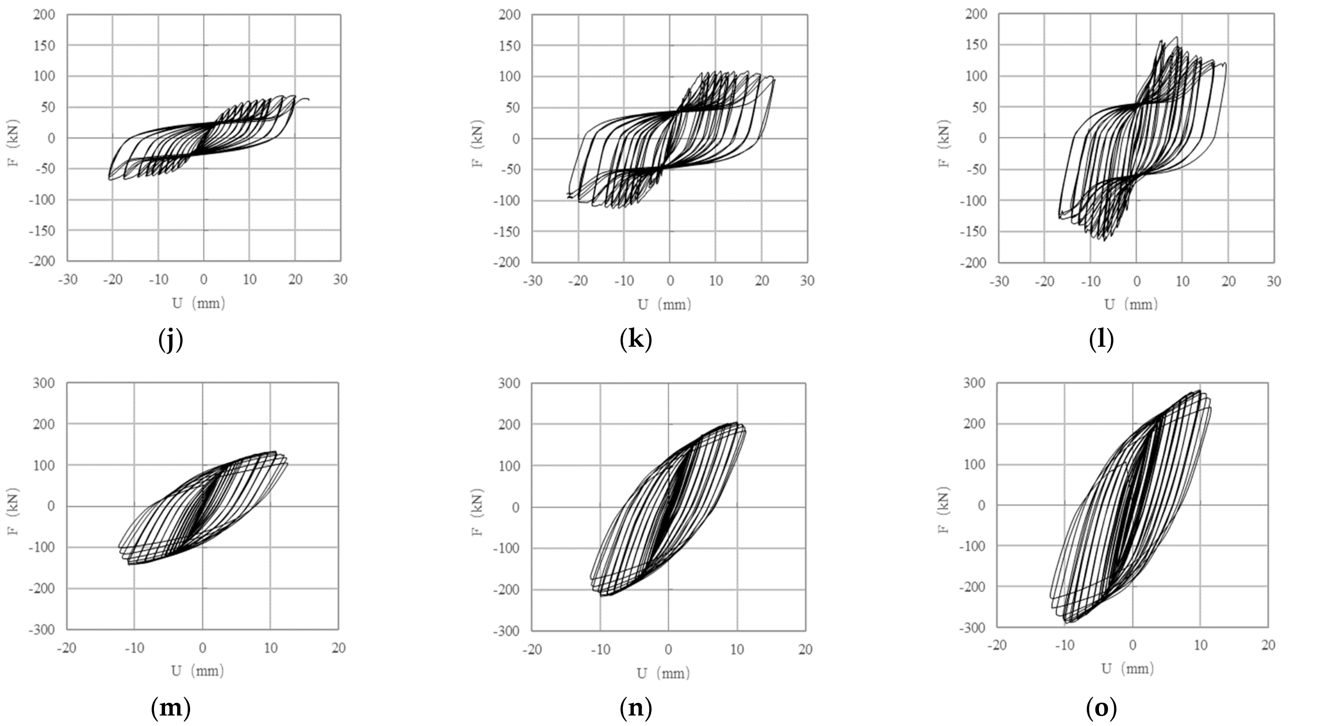

Figure 9. Hysteresis curves of the specimens. (**a**) 150−A1, (**b**) 150−A2, (**c**) 150−A3, (**d**) 150−B1, (**e**) 150−B2, (**f**) 150−B3, (**g**) 150−C1, (**h**) 150−C2, (**i**) 150−C3, (**j**) 150−D1, (**k**) 150−D2, (**l**) 150−D3, (**m**) 200−A1, (**n**) 200−A2, (**o**) 200−A3.

It can be observed from Figure 9 that:

1. The hysteretic curves of specimens 150-A1, 150-A2, and 150-A3 were fusiform, and with increasing width, the hysteretic curves of the shear square steel tube dampers gradually grew full, and the energy dissipation capacities of the dampers were enhanced. When the damper reached peak load, the load-bearing capacity gradually decreased. Before the load-bearing capacity dropped, the hysteretic curves of the dampers were relatively full, indicating that the dampers' energy dissipation capacity is strong.
2. The hysteretic curves of specimens 150-B1, 150-B2, and 150-B3 were in the shape of fusions, and the hysteretic curves of specimen 150-B3 appeared as a slight buckling phenomenon, which may be caused by the out-of-plane buckling of the steel tube due to the lack of out-of-plane constraints. With increasing width, the hysteretic curves of the specimens gradually grew full, and the energy dissipation capacities of the dampers were enhanced. Before the load-bearing capacity dropped, the hysteretic curves of the dampers were relatively full, indicating the dampers' strong energy dissipation capacity. After the load-bearing capacity reached the maximum, it decreased rapidly and soon lost its working capacity.
3. The hysteretic curves of specimens 150-C1, 150-C2, and 150-C3 were full, with a shape close to the parallelogram, and reflected good energy dissipation capacity. With increasing width, the hysteretic curves of the specimens gradually became full, and the energy dissipation capacities of the specimens increased. The positive and negative loads of the damper were not the same, which may have been due to an error in installation. All three specimens showed slight pinching, which was caused by out-of-plane buckling due to the lack of out-of-plane constraints on the steel tube. Comparing the specimens 150-A, 150-B, and 150-C, when other parameters were the same, the greater the steel tube thickness was, the greater the load-bearing capacity of the dampers was, and the greater the hysteresis loop area was.

4. The hysteretic curves of specimens 150-D1, 150-D2, and 150-D3 were Z-shaped. After the damper yielded, it could remain at high load for a period. Because the corner of the steel tube of the bolted damper warped at late loading, there was no obvious growth of the horizontal peak load. In the middle of the hysteretic curve, displacement grew without obvious growth of the horizontal load.
5. The hysteretic curves of specimens 200-A1, 200-A2, and 200-A3 were fusiform and reflected good energy dissipation capacity. The wider the curves were, the fuller they were, and the more energy was dissipated from the corresponding specimens. Compared with the specimen 150-C, the specimens with heights of 200 mm had greater ultimate displacement, but their load-bearing capacity was lower.

3.4. Skeleton Curves and Stiffness Degradation Curves

The skeleton curve of each specimen is shown in Figure 10.

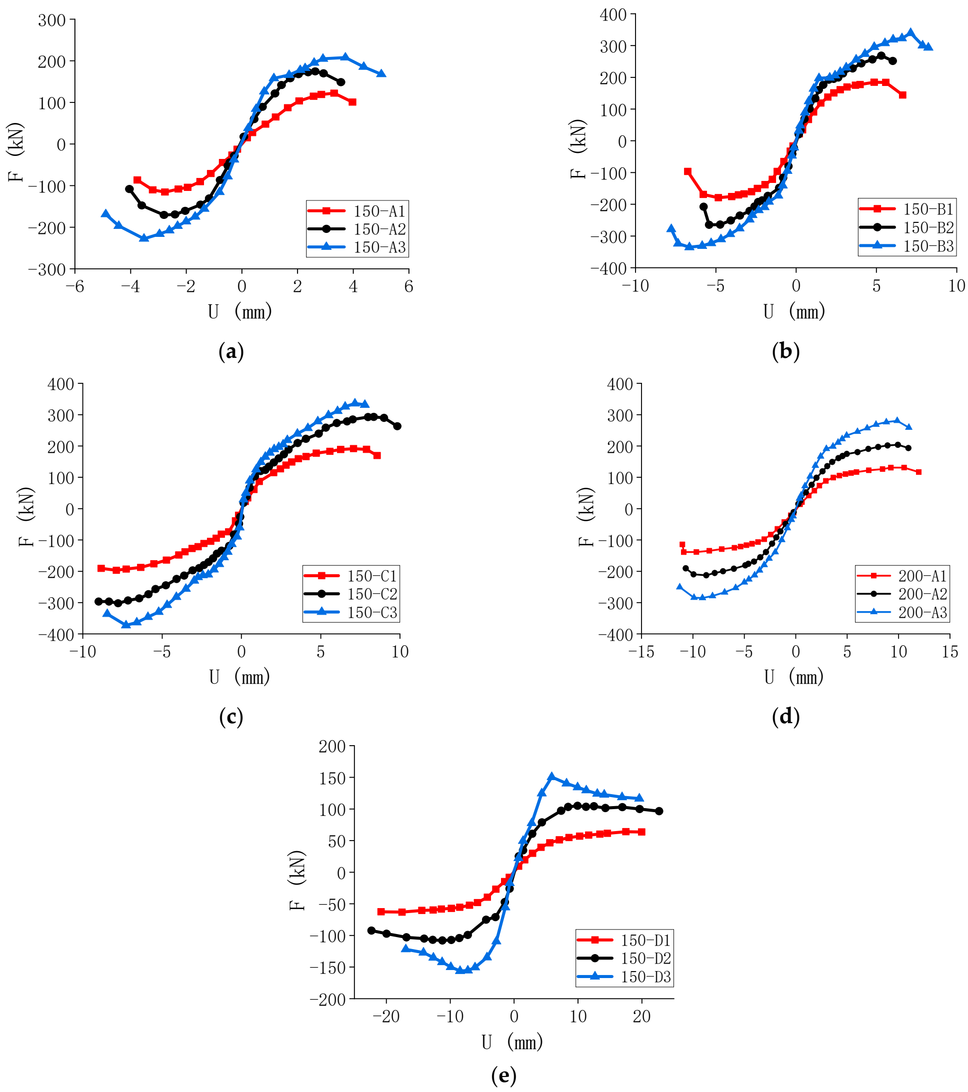

Figure 10. Skeleton curves of the specimens (**a**) 150-A, 150-A2, and 150-A3; (**b**) 150-B1, 150-B2, and 150-B3; (**c**) 150-C1, 150-C2, and 150-C3; (**d**) 200-A1, 200-A2, and 200-A3; (**e**) 150-D1, 150-D2, and 150-D3.

Equivalent stiffness K is the slope of the line between the origin and the load-bearing capacity peak point of each circle of hysteretic curves, which can reflect the change in stiffness. The formula for equivalent stiffness is

$$K = \frac{|+P_\mathrm{i}| + |-P_\mathrm{i}|}{|+\Delta_\mathrm{i}| + |-\Delta_\mathrm{i}|}$$

where P_i is the peak load of the circle I and Δ_i is the displacement corresponding to the load P_i. The stiffness degradation curve of each specimen is shown in Figure 11.

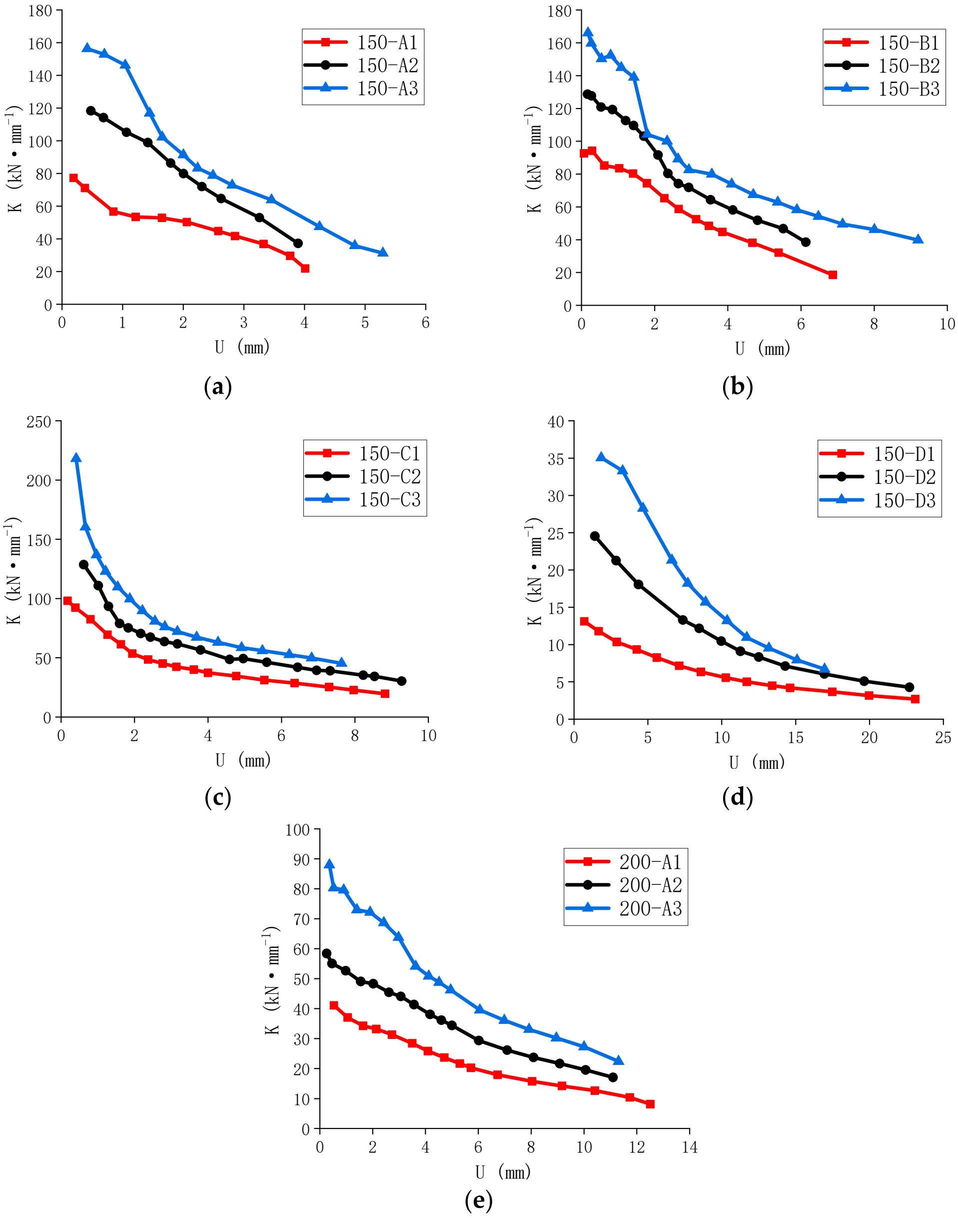

Figure 11. Skeleton curves of the specimens (**a**) 150–A, 150–A2, and 150–A3; (**b**) 150–B1, 150–B2, and 150–B3; (**c**) 150–C1, 150–C2, and 150–C3, (**d**) 150–D1, 150–D2, and 150–D3; (**e**) 200–A1, 200–A2, and 200–A3.

It can be seen from Figures 10 and 11 that:

1. Comparing all the specimens, the wider the steel tube was, the greater the equivalent stiffness was. With increasing displacement, the equivalent stiffness of all three specimens showed a downward trend.

2. The equivalent stiffness degradation curve of 150−A2 was almost linear throughout the whole process, and the stiffness degradation range of 150-A1 and 150-A3 at the initial stage was slightly higher than that at the later stage of loading.
3. For specimens 150−C1, 150−C2, and 150−C3, the stiffness degradation at the initial stage of loading was significantly higher than that at the later stage of loading. Moreover, the greater the initial stiffness was, the more obvious the stiffness degradation was.
4. Comparing specimens in group 150-C (with welded connections) with the specimens of the same size in group 150−D (with bolted connections), the stiffness of the welded dampers was always greater than that of the bolted dampers under the same displacement.

3.5. Energy Dissipation

The energy dissipation of a specimen can reflect its ability to dissipate seismic energy in an earthquake to reduce the seismic response of the main structure. The area enclosed by the hysteretic curves of the damper can reflect the absorbed and dissipated energy, so the energy dissipation capacity of the damper can be reflected by the area of the hysteretic loops. The sum of the hysteresis loop area and the equivalent viscous damping coefficients of specimens from the beginning of loading to the final failure mode are shown in Table 4. The hysteresis loop area was calculated by Origin software. The force and displacement data were imported into the software to draw the hysteresis curve, and the hysteresis loop area was calculated by the software. The equivalent viscous damping coefficient is equal to the area of the hysteretic curve divided by the nominal elastic potential energy, which is equal to the product of the yield displacement and the yield load. Generally, in order to simplify the calculation, the Chinese specifications "Specification for seismic test of buildings" JCJ/T 101–2015 were used for the calculation, schematically as follows:

$$\xi = \frac{1}{2\pi} \cdot \frac{S_{\mathrm{ABCD}}}{S_{(\mathrm{OBE+ODF})}}$$

where ξ is the equivalent viscous damping coefficient, S_{ABCD} represents the area of the hysteresis loop, and $S_{(\mathrm{OBE+ODF})}$represents the area of the triangles S_{OBE} and S_{ODF} as shown in Figure 12.

Table 4. Hysteresis loop area of welded seamless steel tube dampers.

Specimens	Energy Dissipation/kN·mm	S_{ABCD}/kN·mm	$S_{(\mathrm{OBE+ODF})}$/kN·mm	Equivalent Viscous Damping Coefficient
150-A1	3905.40	596.75	433.24	0.22
150-A2	7723.53	977.12	553.36	0.28
150-A3	15,795.12	1396.19	854.52	0.26
150-B1	13,978.32	1562.05	934.93	0.27
150-B2	30,195.37	3004.94	1483.52	0.32
150-B3	64,488.01	5406.19	2600.12	0.33
150-C1	48,224.81	3286.22	1686.38	0.31
150-C2	67,790.33	5097.96	2579.84	0.31
150-C3	97,713.07	4169.23	2815.41	0.24
200-A1	36,869.10	2206.40	1248.55	0.28
200-A2	51,116.49	3595.52	2128.33	0.27
200-A3	78,015.56	4939.12	2722.30	0.29
150-D1	22,752.19	1505.28	1155.87	0.21
150-D2	51,914.42	3523.44	2126.96	0.26
150-D3	58,807.43	3907.24	2185.04	0.28

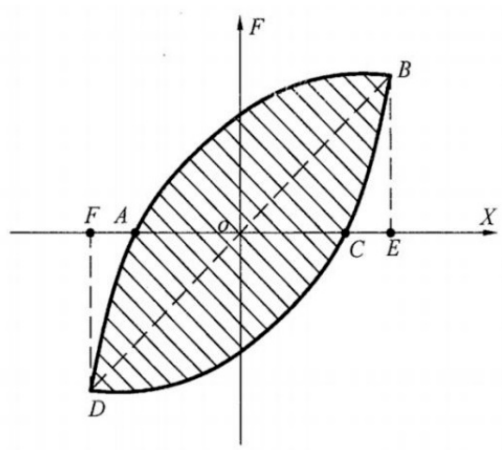

Figure 12. Calculation diagram of equivalent viscous damping coefficient.

It can be observed from Table 4 that:

1. Specimens 150-C1, 150-C2, and 150-C3 had energy dissipation values of 48,224.81 kN·mm, 67,790.33 kN·mm, and 97,713.07 kN·mm, respectively. With increasing steel tube width, the area of the hysteretic loops and the energy dissipation capacity of the dampers gradually increased.
2. Specimens 150-A1, 150-B1, and 150-C1 had energy dissipation values of 3905.40 kN·mm, 13,978.32 kN·mm, and 48,224.81 kN·mm, respectively. This indicates that as the thickness of the steel tube increased, both the area of the hysteretic loops and the energy dissipation of the damper increased.
3. The energy dissipation values for specimens 150-C1 and 200-A1 were 48,224.81 kN·mm and 36,869.10 kN·mm, respectively, showing a reduction of 23.5%. This shows that the longer and the higher the steel tube was, the worse the energy dissipation capacity was.
4. The energy dissipation values for specimens 150-C1 and 150-D1 were 48,224.81 kN·mm and 22,752.19 kN·mm, respectively. The bolted connection mode's energy dissipation value was lower than that of the welded connection mode by 53.82%, indicating that the welded damper could dissipate much more energy.

4. Conclusions

In this paper, the effects of different design parameters on the energy dissipation capacity of the proposed double-sided shear low-cost steel tube damper were explored through experiments. The test phenomena and data were compared and analyzed, and the following conclusions were obtained:

1. The thickness of the steel tube damper and the width of the shear surface had a positive effect on the initial stiffness, and the influence of shear surface width was more significant. Increasing steel tube height had two effects: to increase the yield displacement and peak displacement and to reduce the yield load, peak load, and initial stiffness.
2. The hysteretic curve of each specimen was full, and the energy dissipation capacity is good. After the load-bearing capacity reached the peak load, the load-bearing capacity of each damper decreased rapidly. Comparing the test results of each group, the greater the thickness of the steel tube was, the greater the load-bearing capacity of the damper was, and the larger the hysteresis loop area was. The ultimate displacement of the specimens with high steel tube height was greater, but the load-bearing capacity was reduced.
3. The greater the width of the steel tube was, the greater the equivalent stiffness was. With increasing displacement amplitude, the equivalent stiffness of the specimen showed a downward trend. The initial decline amplitude was significantly higher than that in the later stage of loading. The greater the initial stiffness was, the more

obvious the stiffness degradation was, and the stiffness degradation tended to be gentle in the later stage of the test.

4. With increasing steel tube width and thickness, the hysteretic loop area and the energy dissipation capacity of the specimens gradually increased, while with increasing steel tube height, the energy dissipation and the seismic effect decreased.
5. The welded damper had better yield load, peak load, and initial stiffness, but the bolted damper had greater yield displacement and peak displacement. The bolt connected damper had good ductility and still maintained a good energy dissipation capacity for a period of time after reaching yield and plastic deformation, but the corner of the steel tube tilted up in the later stage of loading, and the peak value of horizontal force did not increase significantly in the later stage. Under the same displacement, the stiffness of the welded damper was always greater than that of the bolted damper, and the welded damper could dissipate more energy. Therefore, a damper with reasonable connection form would need to be selected according to actual engineering needs.

Author Contributions: Conceptualization, L.X. and C.H.; methodology, Y.L.; software, Y.L.; validation, L.X. and C.H.; formal analysis, Z.Z.; investigation, F.D.; resources, Z.Z.; data curation, Z.Z.; writing—original draft preparation, Y.L.; writing—review and editing, C.H.; visualization, Y.L.; supervision, Z.Z.; project administration, Z.Z.; funding acquisition, Z.Z. All authors have read and agreed to the published version of the manuscript.

Funding: This study was funded by the National Key Research and Development Program of China (2019YFC1509304), the Training Plan for Young Key Teachers of the Institution of Higher Education in Henan Province (2019GGJS147), and the Key Scientific Research Project of the Institution of Higher Education in Henan Province (20A560026).

Institutional Review Board Statement: Not applicable.

Informed Consent Statement: Not applicable.

Data Availability Statement: Data are contained within the article.

Conflicts of Interest: The authors declare that they have no known competing financial interests or personal relationships that could have appeared to influence the work reported in this paper.

References

1. Huang, Z.; Li, R.Q.; Yang, L.Z. Study on the Performance-Based Aseismic Design for RC Frame with Mild Steel Shear Damper. *Adv. Mater. Res.* **2014**, *1065–1069*, 1513–1517. [CrossRef]
2. Mirzai, N.M.; Attarnejad, R.; Hu, J.W. Experimental investigation of smart shear dampers with re-centering and friction devices. *J. Build. Eng.* **2021**, *35*, 102018. [CrossRef]
3. Mirzai, N.M.; Attarnejad, R.; Hu, J.W. Analytical investigation of the behavior of a new smart recentering shear damper under cyclic loading. *J. Intell. Mater. Syst. Struct.* **2019**, *31*, 550–569. [CrossRef]
4. Zhu, B.; Wang, T.; Zhang, L. Quasi-static test of assembled steel shear panel dampers with optimized shapes. *Eng. Struct.* **2018**, *172*, 346–357. [CrossRef]
5. Zhao, Y.; Zhang, L. Damage Quantification of Frame-Shear Wall Structure with Metal Rubber Dampers under Seismic Load. *Revue des Composites et des Matériaux Avancés* **2020**, *30*, 227–234. [CrossRef]
6. Wang, B.; Yan, W.; He, H. Mechanical Performance and Design Method of Improved Lead Shear Damper with Long Stroke. *Shock Vib.* **2018**, *2018*, 1–18. [CrossRef]
7. Chen, R.; Xing, G. SEISMIC Analysis of high-rise buildings with composite metal damper. In *MATEC Web of Conferences; Da lian, China*; EDP Sciences: Dalian, China, 2015; Volume 31. [CrossRef]
8. Bakhshayesh, Y.; Shayanfar, M.; Ghamari, A. Improving the performance of concentrically braced frame utilizing an innovative shear damper. *J. Constr. Steel Res.* **2021**, *182*, 106672. [CrossRef]
9. Ghamari, A.; Haeri, H.; Khaloo, A.; Zhu, Z. Improving the hysteretic behavior of Concentrically Braced Frame (CBF) by a proposed shear damper. *Steel Compos. Struct.* **2019**, *30*, 383–392. [CrossRef]
10. Ghamari, A.; Kim, Y.-J.; Bae, J. Utilizing an I-shaped shear link as a damper to improve the behaviour of a concentrically braced frame. *J. Constr. Steel Res.* **2021**, *186*, 106915. [CrossRef]
11. Lin, X.; Wu, K.; Skalomenos, K.A.; Lu, L.; Zhao, S. Development of a buckling-restrained shear panel damper with demountable steel-concrete composite restrainers. *Soil Dyn. Earthq. Eng.* **2019**, *118*, 221–230. [CrossRef]

12. Deng, K.; Pan, P.; Li, W.; Xue, Y. Development of a buckling restrained shear panel damper. *J. Constr. Steel Res.* **2015**, *106*, 311–321. [CrossRef]
13. Yao, Z.; Wang, W.; Zhu, Y. Experimental evaluation and numerical simulation of low-yield-point steel shear panel dampers. *Eng. Struct.* **2021**, *245*, 112860. [CrossRef]
14. Kamaludin, P.; Kassem, M.M.; Farsangi, E.N.; Nazri, F.M.; Yamaguchi, E. Seismic resilience evaluation of RC-MRFs equipped with passive damping devices. *Earthq. Struct.* **2020**, *18*, 391–405. [CrossRef]
15. Aydin, E.; Ozturk, B.; Bogdanovic, A.; Noroozinejad Farsangi, E. Influence of soil-structure interaction (SSI) on optimal design of passive damping devices. *Structures* **2020**, *28*, 847–862. [CrossRef]
16. Cruze, D.; Gladston, H.; Farsangi, E.N.; Loganathan, S.; Dharmaraj, T.; Solomon, S.M. Development of a Multiple Coil Magneto-Rheological Smart Damper to Improve the Seismic Resilience of Building Structures. *Open Civ. Eng. J.* **2020**, *14*, 78–93. [CrossRef]
17. Cruze, D.; Gladston, H.; Farsangi, E.N.; Banerjee, A.; Loganathan, S.; Solomon, S.M. Seismic Performance Evaluation of a Recently Developed Magnetorheological Damper: Experimental Investigation. *Pract. Period. Struct. Des. Constr.* **2021**, *26*, 04020061. [CrossRef]
18. Khalili, M.; Sivandi-Pour, A.; Noroozinejad Farsangi, E. Experimental and numerical investigations of a new hysteretic damper for seismic resilient steel moment connections. *J. Build. Eng.* **2021**, *43*, 102811. [CrossRef]
19. Fathizadeh, S.F.; Dehghani, S.; Yang, T.Y.; Noroozinejad Farsangi, E.; Vosoughi, A.R.; Hajirasouliha, I.; Takewaki, I.; Málaga-Chuquitaype, C.; Varum, H. Trade-off Pareto optimum design of an innovative curved damper truss moment frame considering structural and non-structural objectives. *Structures* **2020**, *28*, 1338–1353. [CrossRef]
20. Dehghani, S.; Fathizadeh, S.F.; Yang, T.Y.; Noroozinejad Farsangi, E.; Vosoughi, A.R.; Hajirasouliha, I.; Málaga-Chuquitaype, C.; Takewaki, I. Performance evaluation of curved damper truss moment frames designed using equivalent energy design procedure. *Eng. Struct.* **2021**, *226*, 111363. [CrossRef]
21. Barbagallo, F.; Bosco, M.; Marino, E.M.; Rossi, P.P.; Stramondo, P.R. A multi-performance design method for seismic upgrading of existing RC frames by BRBs. *Earthq. Eng. Struct. Dyn.* **2017**, *46*, 1099–1119. [CrossRef]
22. Nuzzo, I.; Losanno, D.; Caterino, N. Seismic design and retrofit of frame structures with hysteretic dampers: A simplified displacement-based procedure. *Bull. Earthq. Eng.* **2019**, *17*, 2787–2819. [CrossRef]
23. Mazza, F. A simplified retrofitting method based on seismic damage of a SDOF system equivalent to a damped braced building. *Eng. Struct.* **2019**, *200*, 109712. [CrossRef]
24. Zare Golmoghany, M.; Zahrai, S.M. Improving seismic behavior using a hybrid control system of friction damper and vertical shear panel in series. *Structures* **2021**, *31*, 369–379. [CrossRef]
25. Keykhosro Kiani, B.; Hosseini Hashemi, B. Development of a double-stage yielding damper with vertical shear links. *Eng. Struct.* **2021**, *246*, 112959. [CrossRef]
26. Lin, K.; Zhou, A.; Liu, H.; Liu, Y.; Huang, C. Shear thickening fluid damper and its application to vibration mitigation of stay cable. *Structures* **2020**, *26*, 214–223. [CrossRef]
27. Suzuki, T. Analytical Study on Web Imperfection Design of Shear Panel Damper for Mechanical Performance Control. *J. Struct. Constr. Eng. (Trans. AIJ)* **2019**, *84*, 1401–1409. [CrossRef]
28. Xu, L.-Y.; Nie, X.; Fan, J.-S. Cyclic behaviour of low-yield-point steel shear panel dampers. *Eng. Struct.* **2016**, *126*, 391–404. [CrossRef]